ChemComm

COMMUNICATION

View Article Online
View Journal | View Issue

Cite this: *Chem. Commun.*, 2024, **60**, 3275

Received 19th January 2024,
Accepted 23rd February 2024

DOI: 10.1039/d4cc00279b

rsc.li/chemcomm

Oxygen dynamic exchange and diffusion characteristics of ZnO nanorods from ^{17}O MAS NMR†

Benteng Song,[a] Yuhong Li,*[b] Fang Wang,[a] Yang Wang,[a] Xiaokang Ke[a] and Luming Peng*[a]

Interactions of ZnO nanorods with water and the dynamic migration characteristic of surface oxygen species are important in controlling its structure and catalytic properties. Here, we apply ^{17}O solid-state NMR spectroscopy to investigate the interactions, as well as oxygen ion diffusion properties of ZnO nanorods under different conditions.

ZnO, a technically important metal oxide, has received tremendous interest because of its wide applications in semiconductors,[1] photoelectronics[2] and catalysis.[3,4] For catalytic applications, in particular, the surface structure of ZnO determines its catalytic properties. Detailed structural information is required in order to further improve the performances of the catalyst. Oxygen ions, as the major component of oxide materials, play a very significant role in determining their structural properties and working efficiency. Therefore, the study of the properties of oxygen in oxide crystals, particularly the dynamic exchange and migration characteristics, has attracted increasing attention.[5,6] Traditionally, the investigations of oxygen exchange and diffusion processes in oxides were carried out by ^{18}O–^{16}O isotopic exchange annealing, followed by secondary ion mass spectrometry (SIMS) analysis.[7,8] However, this method involves a number of rapid heating and quenching steps. Not only is this time consuming but also one must exercise great care in order to avoid introducing artefacts and errors into the experimental parameters.[9]

Solid-state magic angle spinning (MAS) NMR spectroscopy is a powerful technique that has been widely used to investigate the composition and the local environments of solids at the atomic level.[10] ^{17}O NMR spectra can give detailed structural information of important functional oxygen-containing materials due to the large chemical shift range (>1000 ppm).[11–14] It is also well suited for investigating the interactions of oxide materials and water (isotopic exchange), as well as oxygen ion migration characteristics in oxides.[15]

The properties of nanocrystals are usually affected by the environment and the working conditions. Among the species that alter the nanocrystals properties, water molecules are of tremendous importance,[16,17] while detailed information on the interactions between the surface and water is still missing. In our previous work,[18] we have revealed the surface structure of ZnO nanorods and distinguished six different types of oxygen ions on the surface and subsurface of ZnO, which provide unprecedented opportunities to further study site-specific interactions of the surface of ZnO nanorods with adsorbed species. In this study, the interactions of ZnO nanorods with water molecules and O ion diffusion properties were investigated by ^{17}O NMR spectroscopy. By adding ^{17}O-enriched water to the sample packed in the NMR rotor, the resulting isotopic exchange process was monitored by ^{17}O NMR in real-time. The changes of NMR spectra after weeks indicate ongoing exchange between the ZnO surface and sorbed H_2O at room temperature. In addition, the diffusion of O ions from the ZnO surface to deeper layers also occurs above 250 °C.

ZnO nanorods were prepared hydrothermally,[19] and transmission electron microscopy (TEM) and X-ray diffraction (XRD) were used to characterize the morphologies and structure. The XRD pattern of the ZnO nanorods confirms that all the diffraction peaks can be indexed to wurtzite ZnO (Fig. S1A, ESI†). The intensity of the $(10\bar{1}0)$ peak, which corresponds to the nonpolar facets, is higher than the (0002) peak, suggesting that this predominantly nonpolar $(10\bar{1}0)$ facet covers the structure, as indicated by the TEM and HRTEM images (Fig. S1B–D, ESI†).

The ^{17}O–^{16}O isotope dynamic exchange between ZnO nanorods and the O atoms from water was monitored by *in situ* ^{17}O

[a] *Key Laboratory of Mesoscopic Chemistry of Ministry of Education and Collaborative Innovation Center of Chemistry for Life Sciences, School of Chemistry and Chemical Engineering, Nanjing University, Nanjing 210023, China. E-mail: luming@nju.edu.cn*

[b] *Suzhou Key Laboratory of Functional Ceramic Materials, School of Materials Engineering, Changshu Institute of Technology, Changshu 215500, Jiangsu Province, China. E-mail: liyh1979@cslg.edu.cn*

† Electronic supplementary information (ESI) available: Experimental section, additional characterization data and experimental NMR spectra. See DOI: https://doi.org/10.1039/d4cc00279b

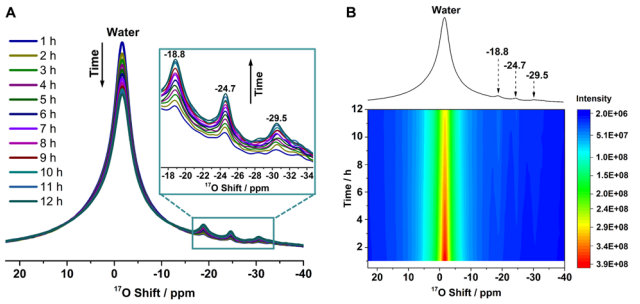

Fig. 1 ^{17}O NMR spectra of the ZnO nanorods. (A) ^{17}O NMR spectra for ZnO nanorods exposed to ^{17}O-enriched water between 1 h and 12 h. (B) Time-resolved ^{17}O NMR spectra of ZnO nanorods with different exposure times to water. The 1D spectrum shown on top corresponds to an exposure time of 4 h. Spectra were obtained at 9.4 T under a MAS rate of 14 kHz, and a recycling delay of 5 s was used.

NMR experiments (Fig. 1A and B), in which 7.5 μL of H_2O enriched in ^{17}O (enrichment degree of 40%) was added to a dry ZnO sample (approx. 35 mg) loaded in a MAS rotor. The ^{17}O NMR spectra show a sharp and intense resonance arising from free water along with three weak peaks at −18.8, −24.7 and −29.5 ppm. The overall ^{17}O–^{16}O isotopic exchange reaction can be represented as $H_2{}^{17}O + Zn^{16}O \rightarrow H_2{}^{16}O + Zn^{17}O$. Based on our previous experimental data and calculations (Fig. S2 and Table S1, ESI†),[18] the peak at −18.8 ppm consists of two components, a broad one corresponding to surface three-coordinated oxygen (O_{3c}) ions in model M2 (ZnO (10$\bar{1}$0) surface with a monolayer of molecularly adsorbed water molecules), and a narrow one arising from subsurface four-coordinated oxygen (O_{4c}) ions in models M2 and M1D1 (ZnO (10$\bar{1}$0) surface with a monolayer of water molecules in which half of the water molecules are dissociatively adsorbed, while the other half molecularly adsorbed). The resonances at −24.7 and −29.5 ppm can be assigned to surface O_{4c} sites in both structures. Fig. 1 shows that the intensity of the peak arising from water molecules decreases over time, while the three resonances centered at −18.8, −24.7 and −29.5 ppm gradually become stronger, indicating that the surface of the ZnO nanorods is very reactive with water and ^{17}O atoms from water can be isotopically exchanged to the ZnO surface.

The decrease in the signal arising from free water in the NMR spectra during the interaction between ZnO nanorods and H_2O is comparable to the increase in the resonances at −18.8, −24.7 and −29.5 ppm (Fig. 1A). The ^{17}O exchange rates, k_1, were determined by monitoring the changes of the ^{17}O NMR signals from ZnO (−18.8, −24.7 and −29.5 ppm) as a function of time according to the expression of the form: $I(t) = I(\infty)\cdot[1 - b\cdot\exp\{-k\cdot t\}]$ where $I(t)$ and $I(\infty)$ denote the intensity of the ^{17}O MAS NMR signals at the time t and in the equilibrium state, respectively, and the value b describes the ^{17}O exchange at $t = 0$.[20] Subsequently, an exchange rate value, k_1, of 0.37 h^{-1} was obtained by data fitting (Fig. S3, ESI†). Note that k_1 corresponds to an apparent exchange rate since several phenomena, such as adsorption of the water molecule, and its diffusion and dissociation, occur on the surface of ZnO and it is also related to the ^{17}O level of water and the surface.[21] Careful analysis indicates that the exchange rates for the three individual resonances are comparable (Fig. S4, ESI†).

Fig. S5 (ESI†) shows the ^{17}O NMR spectra of the ZnO nanorods, obtained from exposing the ZnO nanorods to $H_2{}^{17}O$ at 40 °C for surface-selective labelling,[18] in which the ^{17}O-enriched ZnO sample was named ZnO-W-40-wet and ZnO-W-40 for samples before and after vacuum drying, respectively. The ^{17}O NMR spectrum of ZnO-W-40-wet can be well-fitted with four resonances, including peaks at −18.8, −24.7 and −29.5 ppm owing to surface or subsurface O sites and a broad signal arising from sorbed water at about −2 ppm. After vacuum drying, the peak at −2 ppm disappears, and an ^{17}O signal centered at approx. −52 ppm arises in the ZnO-W-40 sample, which was attributed to hydroxyl species according to its obvious second-order quadrupolar line shape (detailed information can also be seen in our previous work[18]) arising from dissociative adsorption of water on the ZnO surface. The dynamic exchange and diffusion characteristics of O ions in the two samples, ZnO-W-40-wet and ZnO-W-40, will be discussed in the following sections, respectively.

^{17}O NMR spectra further show dynamic exchange of sorbed $H_2{}^{17}O$ with the surface of ZnO-W-40-wet (Fig. 2), in which the amount of sorbed water on the ZnO surface was much smaller than that in Fig. 1 (see Fig. S6 and Table S2, ESI†). The peak at *ca.* −2 ppm assigned to sorbed water decreases significantly with the increase of the intensities of the peaks at −18.8, −24.7 and −29.5 ppm, especially during the first week. In addition, the low-frequency signal ($< \sim -40$ ppm) behaves similarly to the resonance at −2 ppm, which can also be ascribed to sorbed water (detailed information can be seen in Fig. S5 and S7, ESI†). These observations suggest ongoing dynamic exchange between oxygen ions on the ZnO surface and O atoms from water at room temperature for weeks, despite the small amount of $H_2{}^{17}O$ on the ZnO surface. Based on these results, the time dependence of the global ^{17}O signals (integral) for the peaks at −18.8, −24.7

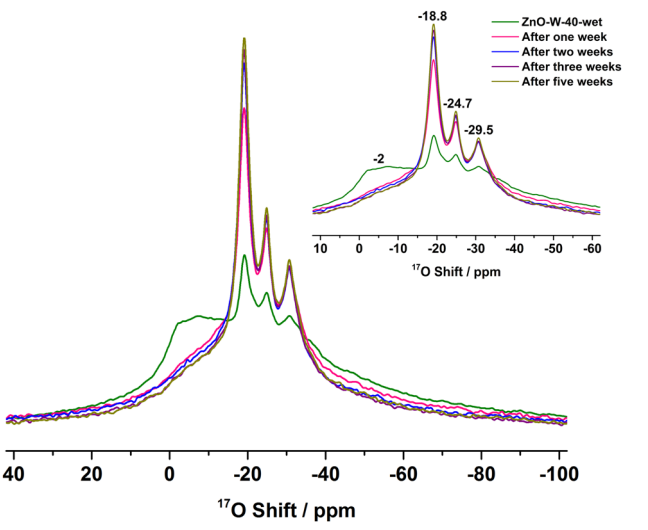

Fig. 2 ^{17}O NMR spectra of ZnO-W-40-wet and ZnO-W-40-wet after being packed in a closed container at ambient temperature for several weeks. All data were obtained at 9.4 T under a MAS frequency of 14 kHz, and recycle delay 5 s was used.

and −29.5 ppm is plotted in Fig. S8 (ESI†), and an apparent exchange rate value, k_2, of 0.15 day^{-1} was obtained, which is much smaller than k_1 presumably due to the decreased difference in the ^{17}O levels of water and the ZnO surface.

In order to reveal the dynamic characteristics of O atoms in ZnO nanorods, we performed the same procedure for ZnO-W-40 as described in ZnO-W-40-wet. Fig. 3A shows that the ^{17}O ZnO signal of hydroxyl species decreases gradually over time with an increase in the resonance at −18.8 ppm. However, the peak at −18.8 ppm may arise from subsurface O_{4c} and/or surface O_{3c}. The surface O_{3c} species is associated with much broader linewidths than subsurface O_{4c} due to larger C_Qs. The difference spectrum, obtained by subtracting the spectrum of the sample directly packed from the spectrum of the sample packed for 5 weeks (Fig. S9, ESI†), shows a narrow peak, indicating that the increase in intensity is mainly due to the increased ^{17}O concentration of subsurface O_{4c}. At the same time, very small or no intensity change is observed for the peak at −24.7 and −29.5 ppm owing to surface O_{4c} sites, and the resonance at −34 ppm (as simulated in Fig. 3B) attributed to the surface O_{3c} site in model M1D1. Therefore, the increase in spectral intensity observed at −18.8 ppm can be ascribed to the diffusion process of O ions located at the surface (*ca.* OH species) into subsurface sites. Obviously, a small diffusion barrier can be expected considering that the diffusion occurs at ambient temperature. The X-ray photoelectron spectroscopy (XPS) spectrum in Fig. S10A (ESI†) shows a large fraction of O vacancies (O_V, 18.9%) on the surface of ZnO-W-40. In addition, the formation energies of O vacancies on the ZnO surface and subsurface sites (Fig. S10B, ESI†) are relatively small, which enables the diffusion of O ions to occur in Fig. 3.

^{17}O solid-state NMR experiments were further carried out to study ZnO-W-40 after thermal treatment to reveal the O migration characteristic in the ZnO nanorods. The ^{17}O NMR spectra in Fig. 4 show a decrease in signal intensities of hydroxyl species along with an increase in peaks at −18.8, −24.7, and −29.5 ppm with increasing temperature in the range of 40 to

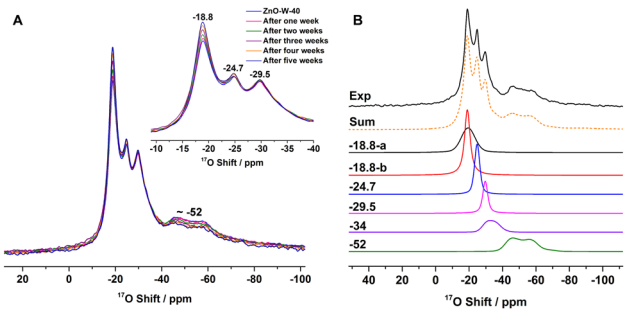

Fig. 3 (A) ^{17}O NMR spectra of ZnO-W-40 and ZnO-W-40 after being packed in a closed rotor at ambient temperature for different times. Spectra were obtained at 9.4 T under a MAS rate of 14 kHz, and recycle delay 5 s was used. (B) The experimental ^{17}O NMR spectra (Exp.) of ZnO-W-40 and the simulated spectra (colored lines and peaks, where −18.8-a, −18.8-b are attributed to the surface O_{3c} sites in model M2 and subsurface O_{4c} sites in both M1D1 and M2 models, respectively; the dashed lines are summation of the simulated peaks) by using parameters obtained from NMR experiments and DFT calculations in our previous work.[18]

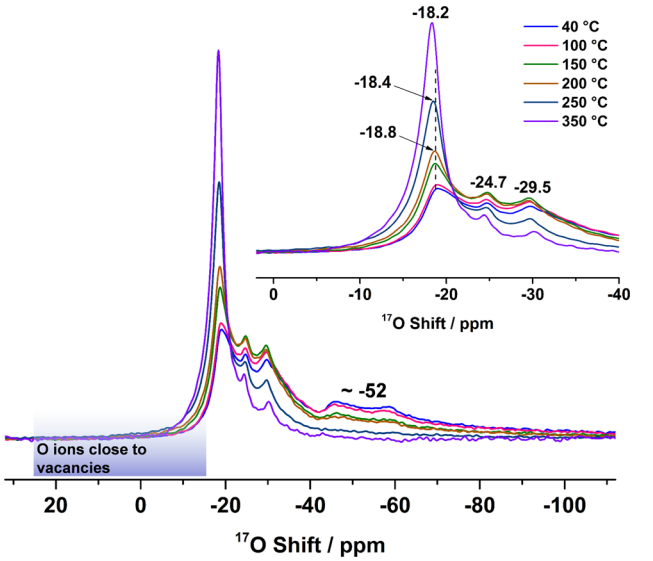

Fig. 4 ^{17}O NMR spectra of ZnO-W-40 and ZnO-W-40 after being heated at 100 °C, 150 °C, 200 °C, 250 °C and 350 °C in a closed container. Note that the ZnO samples were calcined at 400 °C before the enrichment at 40 °C, in order to exclude the effects from sintering in the following thermal treatment at different temperatures. Spectra were obtained at 9.4 T under a MAS rate of 14 kHz, and recycle delay 5s was used.

200 °C, indicating the conversion of partial hydroxyl species to surface or subsurface O sites. In addition, the ^{17}O NMR shift for the peak at −18.8 ppm remains unchanged, indicating minor diffusion of oxygen ions to the bulk in this temperature range. After heating at 250 °C, the peak at −18.8 ppm shifts to −18.4 ppm, which corresponds to inner oxygen species based on our previous observations[18] and becomes much stronger, while the resonances at −24.7, −29.5 ppm and hydroxyl species signal decrease dramatically, implying that the migration of oxygen ions from the surface to the inner layers occurs at 250 °C. The electron paramagnetic resonance (EPR) spectrum (Fig. S11, ESI†) shows a large fraction of O vacancies in the ZnO nanorods, which enables the diffusion of O ions from the ZnO surface into deep layers.

In addition, the ^{17}O NMR spectrum shows a broader shoulder at higher frequencies (∼−15 to 25 ppm, Fig. 4), which is ascribed to ^{17}O ions in the top layers close to the newly formed oxygen vacancies, according to previous work.[18] With the heating temperature increased to 350 °C, the peak at −18.4 ppm shifts further to −18.2 ppm and dominates the spectrum along with a stronger shoulder peak (∼−15 to 25 ppm), as well as decreased intensities for the peaks at −24.7 and −29.5 ppm and hydroxyl species, indicating further migration of ^{17}O ions to the bulk from all of the surface sites at this temperature. These results mean that O ion diffusion into ZnO nanorods is significantly affected by working temperature.

In summary, we investigated two oxygen migration behaviours during the $H_2{}^{17}O$–ZnO interactions with ^{17}O NMR, namely, surface dynamic exchange and subsurface diffusion (Fig. 5). A rapid exchange process between the ZnO nanorods and water is evidenced in real-time. The surface of ZnO is very

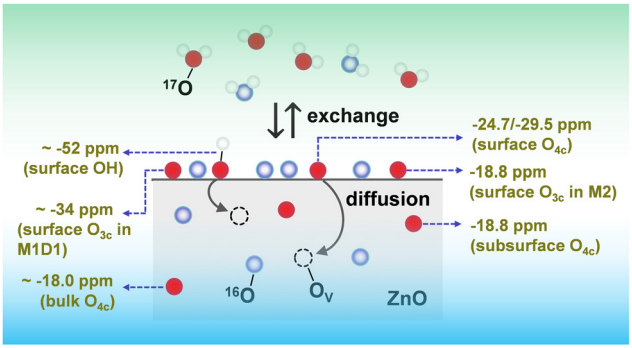

Fig. 5 Schematic diagram for ^{17}O–^{16}O isotope dynamic exchange between ZnO nanorods and ^{17}O-enriched water, as well as the O ion diffusion process from the ZnO surface into deep layers. The ^{17}O signals labelled in the scheme are obtained at 9.4 T. The dashed circles represent oxygen vacancies (O_V). Red, light blue and white spheres represent ^{17}O, ^{16}O, and H atoms, respectively.

reactive with water that plays a vital role in determining the properties of oxides. The isotopic exchange between water and the surface of ZnO due to sorbed $H_2{}^{17}O$ can occur at ambient temperature for weeks, generating an observable ^{17}O NMR signal increase. The rapid cleavage of the ZnO bond and the formation of active hydroxyls should be important for catalytic reactions on the surface of ZnO. For the ZnO-W-40 sample, the surface O species (OH) can migrate into subsurface sites even at ambient temperature. Subsequently, ^{17}O NMR spectra of ZnO-W-40 after different thermal treatment temperatures show that surface O ions can diffuse into deeper layers gradually above 250 °C as indicated by the shift of the peak from −18.8 to −18.2 ppm and its increased peak intensity. This indicates that ^{17}O solid-state NMR spectroscopy is an effective method to probe the dynamic and migration properties of O ions in oxides. The oxygen diffusion behaviours of ZnO at elevated temperatures are worth further investigating since these properties are essential for the use of ZnO in solid oxide fuel cells.[22,23]

This work was supported by the National Key R&D Program of China (2021YFA1502803), the National Natural Science Foundation of China (NSFC) (22272075, 21972066 and 91745202), NSFC – Royal Society Joint Program (21661130149). L. P. thanks the Royal Society and Newton Fund for a Royal Society – Newton Advanced Fellowship. This work was also supported by the Research Funds for the Frontiers Science Center for Critical Earth Material Cycling, Nanjing University and a Project Funded by the Priority Academic Program Development of Jiangsu Higher Education Institutions.

Conflicts of interest

There are no conflicts to declare.

Notes and references

1 F.-R. Fan, Y. Ding, D.-Y. Liu, Z.-Q. Tian and Z. L. Wang, *J. Am. Chem. Soc.*, 2009, **131**, 12036–12037.
2 D. Chen, X. Zou, F. Dong, C. Zhen, D. Xiao, X. H. Wang, Q. Wu, Y. Cao and J. C. Tu, *ACS Appl. Mater. Interfaces*, 2021, **13**, 33006–33014.
3 X. Y. Liu, M.-H. Liu, Y.-C. Luo, C.-Y. Mou, S. D. Lin, H. K. Cheng, J.-M. Chen, J.-F. Lee and T.-S. Lin, *J. Am. Chem. Soc.*, 2012, **134**, 10251–10258.
4 M.-H. Liu, Y.-W. Chen, T.-S. Lin and C.-Y. Mou, *ACS Catal.*, 2018, **8**, 6862–6869.
5 M. Lira-Cantu, K. Norrman, J. W. Andreasen and F. C. Krebs, *Chem. Mater.*, 2006, **18**, 5684–5690.
6 H. J. M. Bouwmeester, C. L. Song, J. J. Zhu, J. X. Yi, M. V. S. Annaland and B. A. Boukamp, *Phys. Chem. Chem. Phys.*, 2009, **11**, 9640–9643.
7 V. Thoréton, M. Niania and J. Kilner, *Phys. Chem. Chem. Phys.*, 2021, **23**, 2805–2811.
8 M. Lira-Cantu, K. Norrman, J. W. Andreasen and F. C. Krebs, *Chem. Mater.*, 2006, **18**, 5684–5690.
9 R. A. D. Souza and R. J. Chater, *Solid State Ionics*, 2005, **176**, 1915–1920.
10 Y.-K. Peng, L. Ye, J. Qu, L. Zhang, Y. Y. Fu, I. F. Teixeira, I. J. McPherson, H. Y. He and S. C. E. Tsang, *J. Am. Chem. Soc.*, 2016, **138**, 2225–2234.
11 N. Kim and C. P. Grey, *Science*, 2002, **297**, 1317–1320.
12 L. M. Peng, Y. Liu, N. Kim, J. E. Readman and C. P. Grey, *Nat. Mater.*, 2005, **4**, 216–219.
13 N. Merle, J. Trébosc, A. Baudouin, I. D. Rosal, L. Maron, K. Szeto, M. Genelot, A. Mortreux, M. Taoufik, L. Delevoye and R. M. Gauvin, *J. Am. Chem. Soc.*, 2012, **134**, 9263–9275.
14 J. C. Chen, F. Wang, Y. J. Wen, W. P. Tang and L. M. Peng, *ACS Catal.*, 2023, **13**, 3485–3500.
15 M. Wang, X.-P. Wu, S. J. Zheng, L. Zhao, L. Li, L. Shen, Y. X. Gao, N. H. Xue, X. F. Guo, W. X. Huang, Z. H. Gan, F. Blanc, Z. W. Yu, X. K. Ke, W. P. Ding, X.-Q. Gong, C. P. Grey and L. M. Peng, *Sci. Adv.*, 2015, **1**, e1400133.
16 M. Daté, M. Okumura, S. Tsubota and M. Haruta, *Angew. Chem., Int. Ed.*, 2004, **43**, 2129–2132.
17 B. Dargatz, J. Gonzalez-Julian and O. Guillon, *J. Cryst. Growth*, 2015, **419**, 69–78.
18 B. T. Song, Y. H. Li, X.-P. Wu, F. Wang, M. Lin, Y. H. Sun, A.-P. Jia, X. Ning, L. Jin, X. K. Ke, Z. W. Yu, G. Yang, W. H. Hou, W. P. Ding, X.-Q. Gong and L. M. Peng, *J. Am. Chem. Soc.*, 2022, **144**, 23340–23351.
19 L. Lin, Y. C. Yang, L. Men, X. Wang, D. He, Y. C. Chai, B. Zhao, S. Ghoshroy and Q. Tang, *Nanoscale*, 2013, **5**, 588–593.
20 X. M. Sun, M. Dyballa, J. Q. Yan, L. Q. Li, N. J. Guan and M. Hunger, *Chem. Phys. Lett.*, 2014, **594**, 34–40.
21 Y. Champouret, Y. Coppel and M. L. Kahn, *J. Am. Chem. Soc.*, 2016, **138**, 16322–16328.
22 M. Chen, Y. M. Guo, J. G. Xu, J. J. Wu and X. Tang, *ACS Appl. Nano Mater.*, 2024, **7**, 628–637.
23 M. A. K. Y. Shah, N. Mushtaq, S. Rauf, C. Xia and B. Zhu, *Int. J. Hydrogen Energy*, 2019, **44**, 30319–30327.

